https://doi.org/10.5607/en.2018.27.2.88
Exp Neurobiol. 2018 Apr;27(2):88-93.
pISSN 1226-2560 • eISSN 2093-8144

Short Communication

Experimental Neurobiology

Electrophysiological Evidence for Functional Astrocytic $P2X_3$ Receptors in the Mouse Trigeminal Caudal Nucleus

Jaekwang Lee[1,2], Jin Young Bae[3], C. Justin Lee[2]* and Yong Chul Bae[3]*

[1]Division of Functional Food Research, Korea Food Research Institute, Jeonju 55365,
[2]Center for Neuroscience and Functional Connectomics, Korea Institute of Science and Technology, Seoul 02792,
[3]Department of Anatomy and Neurobiology, School of Dentistry, Kyungpook National University, Daegu 41940, Korea

Recently, we reported that astrocytes in the trigeminal caudal nucleus (Vc) of the brain stem express a purinergic receptor $P2X_3$, which is involved in the craniofacial pathologic pain. Although we observed protein expression of $P2X_3$ receptors ($P2X_3$ Rs) in the astrocyte of the Vc, it is still unclear that astrocyte has functional $P2X_3$Rs in Vc. To address this issue, we recorded asrtocytic $P2X_3$Rs by using whole cell voltage-clamp recording in the Vc of the GFAP-GFP mice, which was used as a guide to astrocytes with green fluorescence. While measuring voltage ramp-induced astrocytic membrane current, we found the amplitude of the current was increased when we applied P2-purinoreceptor agonist, α,β-meATP. This increase was blocked by co-application of A317491, $P2X_3$R antagonist. These results demonstrate that astrocytes in the Vc express functional $P2X_3$Rs, which might be critical in craniofacial pathologic pain.

Key words: Electrophysiology, Trigeminal Caudal Nucleus, Astrocytes, Purinergic $P2X_3$, Pain

INTRODUCTION

P2X receptor family consists of cation-permeable ligand-gated ion channels that open in response to the binding of extracellular adenosine 5'-triphosphate (ATP). P2X receptors are present in a diverse array of organisms in mice and humans [1]. ATP released from damaged or inflamed tissues can act at P2X receptors expressed on primary afferent neurons [2-4]. The resulting depolarization can initiate action potentials that are interpreted centrally as pain. Among those receptors, $P2X_3$ is sensitive to ATP which is released during tissue injury and has a critical role in peripheral pain response as well as in several signaling pathways involving neuron-glia interaction [5-7]. Astrocytes are implicated in pathological pain associated with nerve injury and inflammation [8-11]. Recently, we reported that 1) astrocytes express $P2X_3$ receptor ($P2X_3$R) in the trigeminal caudal nucleus (Vc), which is a first relay nucleus for the craniofacial nociception in the brain stem and implicated in the neuropathic pain and that 2) the density of astrocytic $P2X_3$R in the Vc is increased following chronic constriction injury of infraorbital nerve (CCI-ION). These findings suggest that astrocytic $P2X_3$R-mediated mechanism is involved in the craniofacial neuropathic pain signaling [12]. Although these findings strongly imply astrocytic $P2X_3$R-involved mechanism in the

Received March 31, 2018, Revised April 12, 2018,
Accepted April 12, 2018

*To whom correspondence should be addressed.
C. Justin Lee, TEL: 82-2-958-6940, FAX: 82-2-958-6937
e-mail: cjl@kist.re.kr
Yong Chul Bae, TEL: 82-53-660-6860, FAX: 82-53-425-6025
e-mail: ycbae@knu.ac.kr

neuropathic pain, there is a lack of direct evidence for functional $P2X_3R$ in the Vc.

To address this issue, we investigated the activity of $P2X_3R$ in astrocytes in the Vc using whole cell voltage-clamp recordings while applying voltage ramp protocol. In this study, we report, for the first time, a functional expression of $P2X_3R$ in the astrocyte of the Vc, which may be involved in the regulation of neuronal activity in pathologic pain condition.

MATERIALS AND METHODS

Animals and tissue preparation

Three male Sprague-Dawley rats, weighing 290~310 g, were used for this study. All animal procedures were reviewed and approved by the Kyungpook National University Intramural Animal Care and Use Committee. The rats were deeply anesthetized with sodium pentobarbital (80 mg/kg, i.p.) and perfused intracardially with 100 ml of heparinized normal saline (0.9% NaCl solution), followed by 500 ml of freshly prepared fixative, a mixture of 4% paraformaldehyde and 0.01% glutaraldehyde in 0.1 M phosphate buffer (PB), pH 7.4 (PB). Brainstem including trigeminal caudal nuclues (Vc) was removed, postfixed in the same fixative for 2 hours at 4°C, and rinsed in PB. Sections were transversely cut on a Vibratome at 60 μm and cryoprotected in 30% sucrose in PB overnight at 4°C.

Electron microscopic preembedding immunohistochemistry

For double immunostaining for $P2X_3$ and GFAP, sections of Vc were frozen on dry ice for 20 minutes, thawed in phosphate-buffered saline (PBS; 0.01 M, pH 7.4) to enhance penetration, and pretreated with 1% sodium borohydride for 30 minutes to remove glutaraldehyde. Sections were then blocked with 3% hydrogen peroxide for 10 minutes, to suppress endogenous peroxidase, and with 10% normal donkey serum (NDS, Jackson ImmunoResearch, West Grove, PA) for 30 minutes, to quench secondary antibody binding sites. Sections were incubated overnight in a mixture of rabbit anti-$P2X_3$ (1:200; Alomone Labs Ltd., Cat. no. APR-016) antibody and mouse GFAP (1:5000, Chemicon, Cat. no. MAB360) antibody in PBS. After rinsing in PBS, sections were incubated with a mixture of biotinylated donkey anti-mouse (1:200, Jackson ImmunoResearch) and 1 nm gold-conjugated donkey anti-rabbit (1:50, EMS, Hatfield, PA) antibodies for 2 hours. The sections were postfixed with 1% glutaraldehyde in PB for 10 minutes, rinsed in PB several times, incubated for 4 minutes with HQ silver enhancement solution (Nanoprobes, Yaphank, NY), and rinsed in 0.1 M sodium acetate and PB. After rinsing, sections were incubated with ExtrAvidin peroxidase (1:5000; Sigma-Aldrich) for 1 hour and the immunoperoxidase was visualized with nickel-intensified 3,3'-diaminobenzidine tetrahydrochloride (DAB). Then, sections were further rinsed in PB, osmicated in 1% osmium tetroxide (in PB) for 1 hour. Sections were further dehydrated in graded alcohols, flat-embedded in Durcupan ACM (Fluka, Buchs, Switzerland) between strips of Aclar plastic film (EMS, Hatfield, PA), and cured for 48 hours at 59°C. Small pieces containing immunostaining for $P2X_3$ and GFAP in Vc were cut out of wafers and glued onto blank resin blocks with cyanoacrylate. Thin sections were cut with a diamond knife, mounted on formvar-coated single slot nickel grids, and stained with uranyl acetate and lead citrate. Grids were examined on a Hitachi H 7500 electron microscope (Hitachi, Tokyo, Japan) at 80 kV accelerating voltage. Images were captured with Digital Micrograph software driving a cooled CCD camera (SC1000; Gatan, Pleasanton, CA) attached to the electron microscope, and saved as TIFF files.

For the quantitative analysis of the $P2X_3$ expression in the astrocytic soma and process, 60 electron micrographs (at 25,000 original magnification) were taken in each section of the Vc from each of three rats. Gold particle density (number of gold particles/μm^2) for $P2X_3$ in the $GFAP^+$ astrocytic soma and process in each rat was measured using a digitizing tablet and Image J software (v.1.45; NIH, Bethesda, MD). Statistical analysis of differences between astrocytic soma and process was performed with Student's t-test.

Slice preparation and electrophysiology

Coronal mouse brain slices (200~300 μm) containing trigeminal caudal nucleus region were acutely prepared from adult GFAP-GFP mice (age 4~8 weeks). Following decapitation the brain was rapidly removed and placed in cold artificial cerebrospinal fluid (ACSF) having the following composition (in mM): 130 NaCl, 24 $NaHCO_3$, 3.5 KCl, 1.25 NaH_2PO_4, 1 $CaCl_2$, 3 $MgCl_2$ and 10 glucose, pH 7.4; room temperature with oxygenation (95% O_2 and 5% CO_2). The slices were made using an oscillating tissue slicer (Linear Slicer) at 4°C and stored in room temperature with oxygenation (95% O_2, 5% CO_2) and prepared slices were left to recover for at least 1 hour before recording. Each slice that was studied was transferred from a recovery/holding reservoir to the recording chamber of a fixed-stage upright microscope (Zeiss Axio Examiner) and submerged in oxygenated ACSF that was supplied to the chamber at a rate of 1.5~2 ml/min. The submerged slice was visualized either directly via the microscope's optics, or indirectly via a high resolution CCD camera system (Orca Flash 2.1, Hamamatsu) that received the output of a CCD camera attached to the microscope's video port. Experiments with a holding current of more than -100 pA or in which there was a change in input resistance >30% of the control were rejected. Recordings were obtained

using Multiclamp 700A (Axon Instruments) and were filtered at 1~2 kHz. Current recordings under ramp protocol were digitized at 5 kHz and analyzed using pCLAMP 10 software (Axon Instruments). Whole-cell recordings from trigeminal astrocyte were carried out with KCl based internal solution composed of (mM): 140 KCl, 2 $MgCl_2$, 10 EGTA, 10 HEPES, 4 MgATP, 0.3 Na_3-GTP and pH 7.2 (OSM=304).

Light microscopic immunohistochemistry

Animals were deeply anesthetized using 2% avertin and perfused with 0.1 M PBS, followed by 4% paraformaldehyde. Brains were postfixed in 4% paraformaldehyde at 4°C for 24 hr and 30% sucrose 4°C for 48 hr. Brains were then cut in coronal sections of 30 μm on a cryosection. Sections were blocked in 0.1 M PBS containing 0.3% Triton X-100 (Sigma) and 2% serum (Donkey and Goat mixture, 1:1, Abcam) for 1 hr at room temperature. Primary antibody was then applied at appropriate dilution [Chicken anti-GFAP at 1:1000 (ab4674, Abcam), Rabbit anti-S100β at 1:500 (ab868, Abcam)] and incubated overnight at 4°C. After this, the sections were washed three times in 0.1 M PBS and incubated in secondary antibody [Alexa 555 donkey anti-chicken IgG at 1:500 (ab150170, Abcam), Alexa 488 goat anti-rabbit IgG at 1:500 (ab150077, Abcam) for 2h]. After three rinses in 0.1 M PBS and the sections were mounted on polysine microscopic slide glass (Thermo Scientific) with fluorosheild with DAPI (F6057, Sigma). Images were acquired using a Nikon A1R confocal microscope and analysed with ImageJ software.

In all statistical comparisons, significance was set at *p<0.05 and **p<0.01. All data are presented as the mean±SEM.

RESULTS AND DISCUSSION

We firstly confirmed the expression of $P2X_3R$ in astrocytes in the trigeminal caudal nucleus (Vc) of the brain stem as reported previously [12]. Under the electron microscopic observation, the immunostaining for $P2X_3R$ in the superficial lamina of the Vc was identified by discrete gold-silver particles, easily distinguishable from that for GFAP, which was in the form of amorphous, electron-dense patches of reaction product (Fig. 1). Immunostaining for $P2X_3R$ was observed in the somata and processes of the GFAP-immunopositive ($GFAP^+$) astrocytes (Soma, Fig. 1A, B and process, Fig. 1C, D) in the Vc. Gold particle density for $P2X_3$, representing $P2X_3$ expression level was significantly higher in the astrocytic process than in the astrocytic soma suggesting that expression level of $P2X_3$ is significantly higher in the astrocytic process than in the astrocytic soma (Fig. 1E).

To test whether the $P2X_3Rs$ in the astrocytes in the Vc are functional, we performed whole cell patch clamp recordings from Vc slices. The soma of the astrocytes in the Vc (trigeminal astrocytes) were relatively smaller (approximately 7~8 μm of diameter of

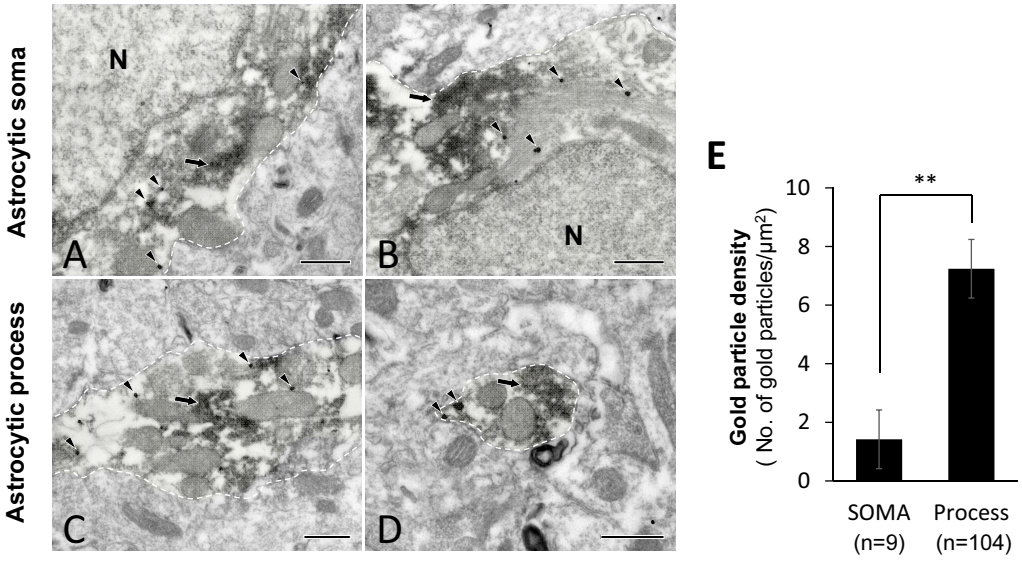

Fig. 1. Electron micrographs showing $P2X_3R$ expression (gold-silver labeling, mostly round black particles) in the GFAP-immunopositive (peroxidase labeling, diffuse darker reaction products) soma (A, B) and processes (C, D) of astrocytes in the brainstem. Arrows indicate immunoperoxidase labeling for GFAP. Arrowheads indicate gold-silver labeling for $P2X_3R$. Astrocytic soma and process are outlined by a dashed line. N= nucleus of astrocyte. Scale bar= 500 nm. (E) Histogram showing gold particle density for $P2X_3$ in the $GFAP^+$ astrocytic soma and process. n= number of astrocytic soma and process analyzed. Asterisk indicates significant differnence between in the $GFAP^+$ astrocytic soma and process at p<0.01.

https://doi.org/10.5607/en.2018.27.2.88

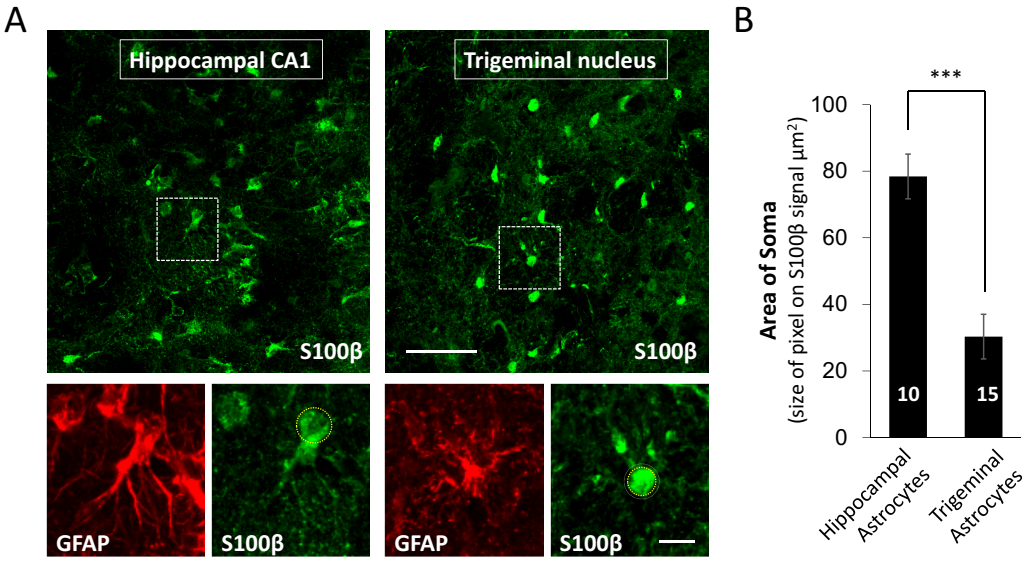

Fig. 2. Comparison of size of soma for astrocytes in hippocampus and trigeminal nucleus. (A) Pictures show result of immunolabeling for GFAP (red) and S100β (green) in hippocampal CA1 and trigeminal nucleus. Upper panel shows low magnification. Lower panel shows high magnification of dotted line box in upper panel. Scale bar indicates 60 μm (upper panel) and 10 μm (lower panel) respectively. (B) Summary bar graph shows area of soma measured pixel size of soma on S100β positive cells in hippocampus and trigeminal astrocyte. ***indicates $p<0.001$ by student t-test.

soma) than that of hippocampal astrocytes when we measured soma area of double positive cells with GFAP and S100β antibodies, both of which are astrocytic marker in CNS (area of soma, size of pixel on S100β signals, μm^2: hippocampal astrocyte, 78.41±6.71, n=10; trigeminal astrocyte, 30.30±0.97, n=15; $p<0.001$, Fig. 2A and 2B). This physical aspect of Vc astrocytes prompted us to use GFAP-GFP mice (mice overexpressing green fluorescent protein under the control of astrocyte-specific GFAP promoter) to visually identify astrocytes in acutely prepared slices. Simultaneously, to enhance chance for tight seal, we used recording electrode with higher pipette resistance (11~14 MΩ) compared with conventional recording electrode (pipette resistance is 4~8 MΩ, which would be ≈ 2 μm pore size of glass electrode). Visual guidance with GFP and smaller tip size of electrode allowed us to identify and successfully whole-cell patch-clamp the astrocytes in Vc (Fig. 3A). To observe ATP-mediated astrocytic current, we monitored the change of membrane conductance stimulated by a periodic voltage ramps from +100 mV to -100 mV and examined both the amplitude of ramp-currents and reversal potentials to verify that recorded-current is mediated by purinergic receptor activity (Fig. 3B). During recordings from astrocyte in the Vc, we found that application of a P2X agonist, α,β-meATP (M6517, Sigma, USA), increased the membrane conductance, and that this effect was blocked by co-application of A317491 (A2979, Sigma, USA), a $P2X_3$ specific antagonist (Fig. 3B and 3C, black and green line). Application of α,β-meATP induced not only increase of amplitude of ramp current, but also induced slow inward current during recordings which was partially blocked by co-application of A-317491 (Fig. 3B). The voltage dependence of $P2X_3$-mediated current was determined by subtracting ramp current traces recorded during co-application of α,β-meATP and A-317491 from those recorded during application of α,β-meATP only (Fig. 3C, blue line). The reversal potential of the $P2X_3$-mediated current fell at around 0 mV, which is consistent with a current mediated by a nonselective cation channel. Summary bar graph showed that application of α,β-meATP increased current density of ramp current in astrocyte and its increase was almost completely blocked by A-317491 (average of pA/pF at maximal peak: Control 29.74±3.75; α,β-meATP, 46.65±5.79; α,β-meATP+A-317491, 32.57±5.28; n=9; $p=0.0227$, Control vs α,β-meATP; $p=0.0029$, α,β-meATP vs α,β-meATP+A-317491, paired sample t-test, Fig. 3D). These results indicate that astrocytes in the Vc express functional purinergic receptors, including $P2X_3$Rs.

In conclusion, we demonstrate for the first time that astrocytes in the Vc express a functional $P2X_3$Rs using whole-cell voltage-clamp recording from trigeminal astrocytes. Together with our previous report that $P2X_3$Rs are upregulated in the fine astrocytic process following CCI-ION [12], this result strongly suggests the existence of astrocytic $P2X_3$R-mediated mechanism for craniofacial neuropathic pain which was initially attributed to neuronal $P2X_3$R on pain sensation. Future investigations on the astrocytic $P2X_3$R-meidated mechanism for the modulation of the primary nociceptive neurons and their postsynatic neurons in the Vc will be needed.

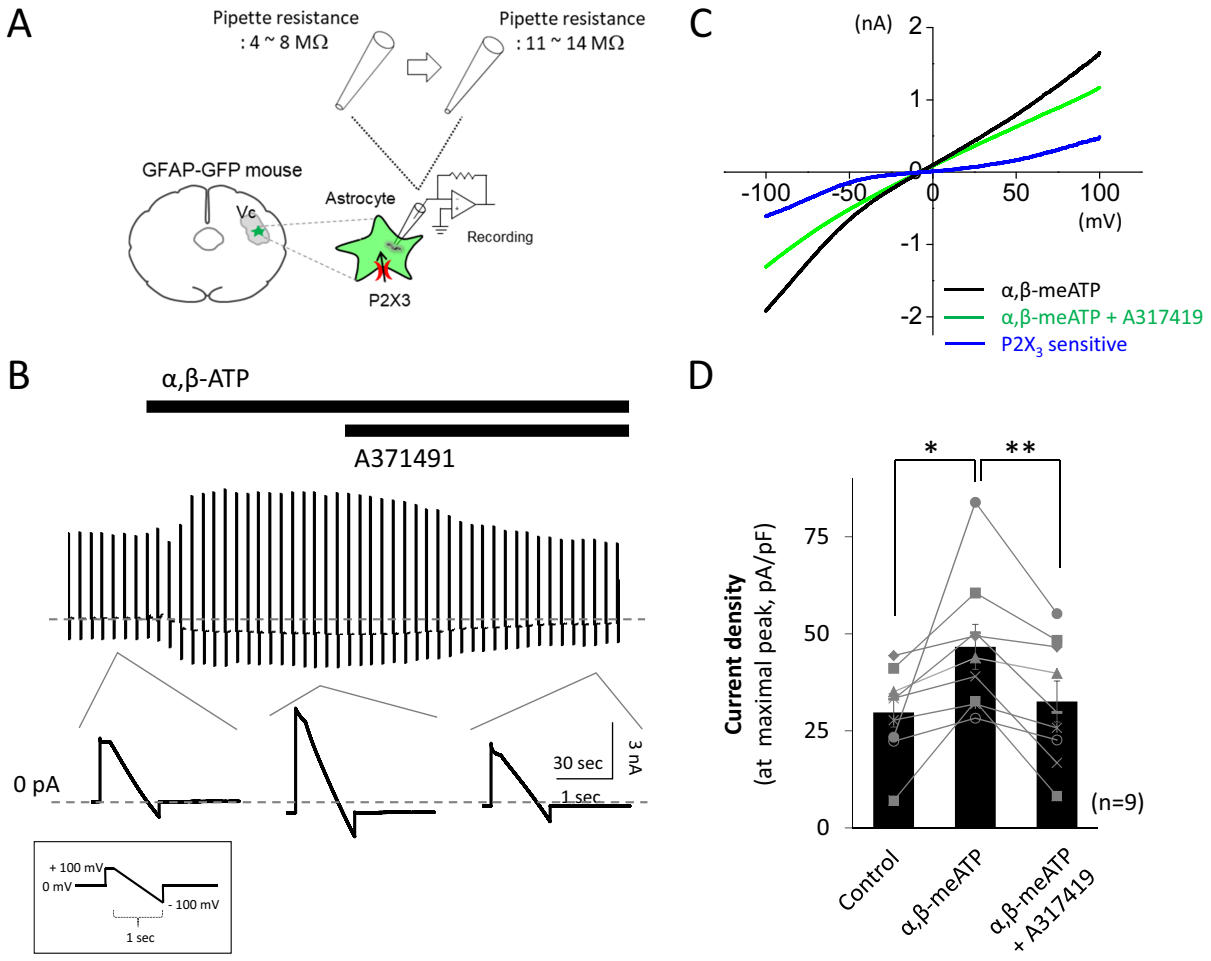

Fig. 3. $P2X_3$ mediated whole cell current was recorded from astrocytes in Vc. (A) Schematic diagram of experimental design for recording astrocyte in Vc. (B) Time course of consecutive ramp current from astrocyte in Vc with application of αβ-meATP and A317491. Lower panel shows representative trace of ramp current baseline, αβ-meATP and A317491 application. Inserted box in below indicates ramp protocol. (C) Representative trace of ramp current from trigeminal astrocyte during application of αβ-meATP (black) and αβ-meATP+A317491 (green). Blue line indicated $P2X_3R$ sensitive current (subtracted from αβ-meATP to αβ-meATP+A317491). (D) Summary bar graph for current density of ramp currents at each condition, * and ** indicate $p<0.05$ and $p<0.01$ respectively, by paired-sample t-test.

ACKNOWLEDGEMENTS

This work was supported by the National Research Foundation of Korea (NRF) grant funded by the Korea government (NRF-2017R1A2B2003561, NRF-2017R1A5A2015391) and by the Korea Health Technology R&D Project through the Korea Health Industry Development Institute (KHIDI), funded by the Ministry of Health & Welfare, Republic of Korea (HI17C0952).

REFERENCES

1. North RA (2002) Molecular physiology of P2X receptors. Physiol Rev 82:1013-1067.
2. Amaya F, Izumi Y, Matsuda M, Sasaki M (2013) Tissue injury and related mediators of pain exacerbation. Curr Neuropharmacol 11:592-597.
3. Cauwels A, Rogge E, Vandendriessche B, Shiva S, Brouckaert P (2014) Extracellular ATP drives systemic inflammation, tissue damage and mortality. Cell Death Dis 5:e1102.
4. Cook SP, McCleskey EW (2002) Cell damage excites nociceptors through release of cytosolic ATP. Pain 95:41-47.
5. Chen CC, Akopian AN, Sivilotti L, Colquhoun D, Burnstock G, Wood JN (1995) A P2X purinoceptor expressed by a subset of sensory neurons. Nature 377:428-431.
6. Chizh BA, Illes P (2001) P2X receptors and nociception. Pharmacol Rev 53:553-568.
7. Dunn PM, Zhong Y, Burnstock G (2001) P2X receptors in peripheral neurons. Prog Neurobiol 65:107-134.

https://doi.org/10.5607/en.2018.27.2.88

8. Chiang CY, Li Z, Dostrovsky JO, Hu JW, Sessle BJ (2008) Glutamine uptake contributes to central sensitization in the medullary dorsal horn. Neuroreport 19:1151-1154.
9. Chiang CY, Wang J, Xie YF, Zhang S, Hu JW, Dostrovsky JO, Sessle BJ (2007) Astroglial glutamate-glutamine shuttle is involved in central sensitization of nociceptive neurons in rat medullary dorsal horn. J Neurosci 27:9068-9076.
10. Okada-Ogawa A, Suzuki I, Sessle BJ, Chiang CY, Salter MW, Dostrovsky JO, Tsuboi Y, Kondo M, Kitagawa J, Kobayashi A, Noma N, Imamura Y, Iwata K (2009) Astroglia in medullary dorsal horn (trigeminal spinal subnucleus caudalis) are involved in trigeminal neuropathic pain mechanisms. J Neurosci 29:11161-11171.
11. Tsuboi Y, Iwata K, Dostrovsky JO, Chiang CY, Sessle BJ, Hu JW (2011) Modulation of astroglial glutamine synthetase activity affects nociceptive behaviour and central sensitization of medullary dorsal horn nociceptive neurons in a rat model of chronic pulpitis. Eur J Neurosci 34:292-302.
12. Mah W, Lee SM, Lee J, Bae JY, Ju JS, Lee CJ, Ahn DK, Bae YC (2017) A role for the purinergic receptor P2X3 in astrocytes in the mechanism of craniofacial neuropathic pain. Sci Rep 7:13627.